



Article

*Currently at: Georg-August-Universität Göttingen, Germany

Cite this article: Westhoff J, Stoll N, Franke S, Weikusat I, Bons P, Kerch J, Jansen D, Kipfstuhl S, Dahl-Jensen D (2021). A stratigraphy-based method for reconstructing ice core orientation. *Annals of Glaciology* 62 (85-86), 191–202. <https://doi.org/10.1017/aog.2020.76>

Received: 8 July 2020

Revised: 10 October 2020

Accepted: 12 October 2020

First published online: 11 November 2020

Keywords:









Glaciological instruments and methods; ice core; structural glaciology

Author for correspondence:

Julien Westhoff,

E-mail: julien.westhoff@nbi.ku.dk

A stratigraphy-based method for reconstructing ice core orientation

Julien Westhoff¹ , Nicolas Stoll² , Steven Franke² , Ilka Weikusat^{2,3} , Paul Bons³ , Johanna Kerch^{2,*} , Daniela Jansen² , Sepp Kipfstuhl^{1,2}  and Dorthe Dahl-Jensen^{1,4} 

¹Physics of Ice, Climate, and Earth, Niels Bohr Institute, University of Copenhagen, Copenhagen, Denmark; ²Alfred Wegener, Institute Helmholtz Centre for Polar and Marine Research, Bremerhaven, Germany; ³Department of Geosciences, Eberhard Karls University Tübingen, Tübingen, Germany and ⁴Centre for Earth Observation Science, University of Manitoba, Winnipeg, Canada

Abstract

Ever since the first deep ice cores were drilled, it has been a challenge to determine their original, in-situ orientation. In general, the orientation of an ice core is lost as the drill is free to rotate during transport to the surface. For shallow ice cores, it is usually possible to match the adjacent core breaks, which preserves the orientation of the ice column. However, this method fails for deep ice cores, such as the EastGRIP ice core in Northeast Greenland. We provide a method to reconstruct ice core orientation using visual stratigraphy and borehole geometry. As the EastGRIP ice core is drilled through the Northeast Greenland Ice Stream, we use information about the directional structures to perform a full geographical re-orientation. We compared the core orientation with logging data from core break matching and the pattern of the stereographic projections of the crystals' *c*-axis orientations. Both comparisons agree very well with the proposed orientation method. The method works well for 441 out of 451 samples from a depth of 1375–2120 m in the EastGRIP ice core. It can also be applied to other ice cores, providing a better foundation for interpreting physical properties and understanding the flow of ice.

1. Introduction**1.1 Why we drill ice cores**

Deep ice core drilling projects are usually undertaken for the purpose of climate reconstruction, which was first demonstrated by Dansgaard and others (1969). The reconstruction of the past climate from ice core samples assumes that the snow in the ice sheet interior does not melt, and that annual layers accumulate horizontally, which leads to a continuous record (Cuffey and Paterson, 2010). The ice flow history can influence the reliability of ice core records and must be considered when reconstructing climate from ice cores (e.g. Jansen and others, 2016). As ice flows, the stratigraphic layers may be disturbed, which can lead to climate reconstruction errors, in particular for the deep parts of the ice column (Dahl-Jensen and others, 2013). Nevertheless, the visualization of stratigraphic deformation offers the possibility to decode past deformation in the bottom part of the ice sheet and to reconstruct ice core orientation.

1.2 Northeast Greenland Ice Stream and EastGRIP drill site

The East Greenland Ice Core Project (EastGRIP or EGRIP) ice core is drilled in northern Greenland (Fig. 1), at 75°38'N, 36°00'W, 2704 m a.s.l. (Vallelonga and others, 2014). This is a central location in the onset region of the Northeast Greenland Ice Stream (NEGIS). The NEGIS extends for more than 600 km almost from the ice divide to the coast. Unlike many ice streams where ice is entering the trunk of fast flow by a tributary system, the ice entering the NEGIS passes through the well-developed shear margins (Fahnestock and others, 2001; Joughin and others, 2001). At the drill site the ice on the surface flows with 55 m/a in an ~10 km wide central flow band (Hvidberg and others, 2020). Observations by Christianson and others (2014) indicate soft and deformable subglacial sediment in the vicinity of the NEGIS, which facilitate sliding as well as a connection of the shear margins' positioning to the subglacial hydrology. Observations by Franke and others (2020) support these findings and indicate the existence of subglacial landforms, shaped by the activity of the ice stream.

1.3 Determining ice core orientation

In the visual stratigraphy images from EastGRIP, milky, impurity rich layers, known as cloudy bands, are found. These were observed and described for the first time by Gow and Williamson (1971) in Antarctica and Hammer and others (1978) in Greenland. These cloudy bands are only visible in ice from the last glacial period, i.e. below a depth of 1375 m (Mojtabavi and others, 2019). All previously drilled ice cores in Greenland show cloudy bands (Faria and others, 2010), but at EastGRIP, rapid changes from perfectly flat cloudy bands in one sample,

© The Author(s), 2020. Published by Cambridge University Press. This is an Open Access article, distributed under the terms of the Creative Commons Attribution licence (<http://creativecommons.org/licenses/by/4.0/>), which permits unrestricted re-use, distribution, and reproduction in any medium, provided the original work is properly cited.

cambridge.org/aog

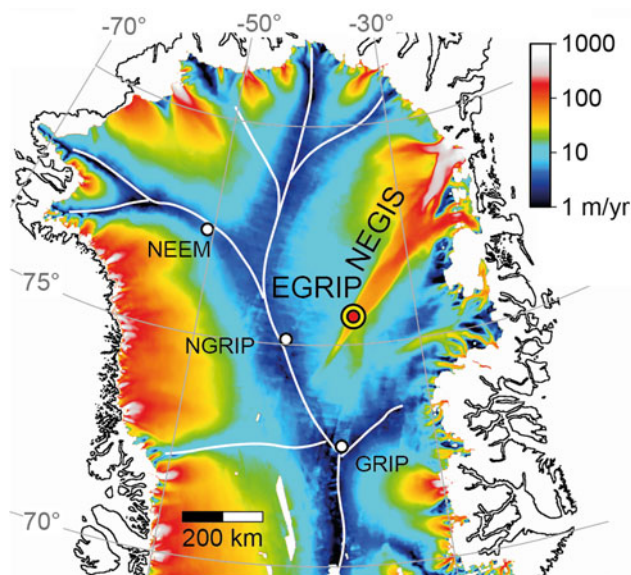


Fig. 1. Surface velocity map of northern Greenland on a logarithmic scale. Locations of the EGRIP drill site in the upper part of NEGIS and other selected ice core drill sites on ice divides (white lines). NEGIS extends almost from the ice divide, Southwest of EastGRIP, to the coast. Surface velocities were obtained from the MEaSURES velocity data set (Joughin and others, 2010a, 2010b, same as used by Bons and others, 2018) with data from the years 2000–2008.

to significantly folded layers in the next sample, were unexpected and unprecedented. These changes tend to occur at core breaks between two samples (sample length: 165 cm), collected in a single drill run. Thus, these features could be a result of randomized and irregular core rotation occurring each time a core section was drilled.

During the process of core recovery, the orientation is lost due to rotation of the drill. See Johnsen and others (2007) for a thorough description of electromechanical ice core drilling. Attempts to preserve this orientation, e.g. by using a spring to guide the drill, failed to work so far (Trevor Popp, pers. comm.).

Borehole logging to determine borehole inclination (also referred to as plunge) and azimuth direction (also referred to as plunge direction) is common practice in ice core and rock drilling. For many methods, it is the first necessary step to retrieve core orientation. Further mechanical devices are required to orient the core fully (Davis and Cowan, 2012). From rock drilling, many methods for reorienting a core are known. Methods such as ‘the spear’, sending a heavy spear with a sharp point or wax-pencil tip downhole after every run that marks the bottom edge of the core (Davis and Cowan, 2012), were not used in ice core drilling due to lack of time in the short drill season in summer and concerns about damage to the ice sample. Furthermore, this method only delivers reliable results in boreholes with an inclination greater than 15°. Many newer methods have evolved over the last decades, such as, Ezy-Mark, Ballmark, and Reflex systems, but have not been applied to ice core drilling. Paulsen and others (2002) describe reorienting features using a downhole camera and matching these to features in the drill core. This is not applicable to EastGRIP, as there are no images of the borehole so far. Downhole imaging has been applied to the upper part (top 630 m) of the North Greenland Eemian Ice Drilling (NEEM) ice core, but not used for determining orientations (Hubbard and Malone, 2013).

First oriented ice cores were drilled with a thermal drill at Vostok Station in 1972 (Talalay, 2020). A horizontal bolt was screwed near the thermal head and melted a groove on the core surface during drilling. An inclinometer section was embedded

in the meltwater tank. Like this, three oriented core sections, of ~1 m each, were recovered. This method works well with thermal drills, as there is no internal rotation of drill sections. It becomes more complicated with electromechanical and thermal cable-suspended drills as the bottom drill parts rotate while drilling.

Recording azimuth and inclination of the non-rotational drill parts at the moment of core breaking are suggested by Talalay (2014). This provides the spatial position of the pressure chamber, which can be related to the rotational parts of the drill section, thus retrieving the core orientation. Fitzpatrick and others (2014) applied this idea and retrieved core orientations relative to magnetic North, which were marked using an azimuth line on the core just before extraction from the drill barrel. These marks did not always line up, either due to rotation of the core in the core barrel (Fitzpatrick and others, 2014) or due to problems with the azimuth measurements (Pavel Talalay, pers. comm.).

1.4 Motivation

In this study, we introduce a new method to determine ice core orientation. The main innovation is the usage of geological drilling know-how, such as the combination of borehole inclination with the apparent layer dip and applying this to directional features visible in ice cores. This is the first time, that directional features are used for thorough and complete reconstruction of ice core orientation.

To understand the flow of ice, we depend on directional information. The spatial orientation of large-scale radar images, showing the ice sheet’s internal structure, is linked to the flight or ground path from which they were acquired. Thus, the direction can readily be implemented. However, due to the loss of ice core orientation during core recovery, all measurements done on an ice core are interpreted without directional information. However, this information about an ice core’s orientation is crucial and a necessity for interpreting physical and flow properties of ice, and all other image data taken from the ice core. If the orientation is known, ambiguous observations are avoided, which allows for a more confident interpretation of the data.

As drills that preserve or record ice core orientation for the entire core have not been applied yet, other methods are required to determine core orientation. The method presented here supplies a technique, independent of the relative orientation obtained during logging by core break-matching (discussed later) and independent of stereographic projections of *c*-axis distribution (Weikusat and others, 2017, also discussed later). We determine the orientation of 451 samples from 1375 to 2120 m depth, i.e. ice from the last glacial period (Mojtabavi and others, 2019), characterized by the occurrence of cloudy bands (Hammer and others, 1978). These cloudy bands are necessary for the application of the method, as well as a certain amount of flow, to detect directional deformation. Additionally, some borehole inclination is necessary, as this method will not provide results in a perfectly vertical borehole, which would be a rare case in the electromechanical ice core drilling. We then compare our results to core break matching and *c*-axis orientations, for verification of our method.

2. Methods

2.1 Journey of an ice core – from the bottom of the ice sheet to the measurement table

During drilling and core preparation, many steps change the orientation of the sample before measurements are made. The drill (Fig. 2a) cuts a cylinder out of the ice, with the bottom

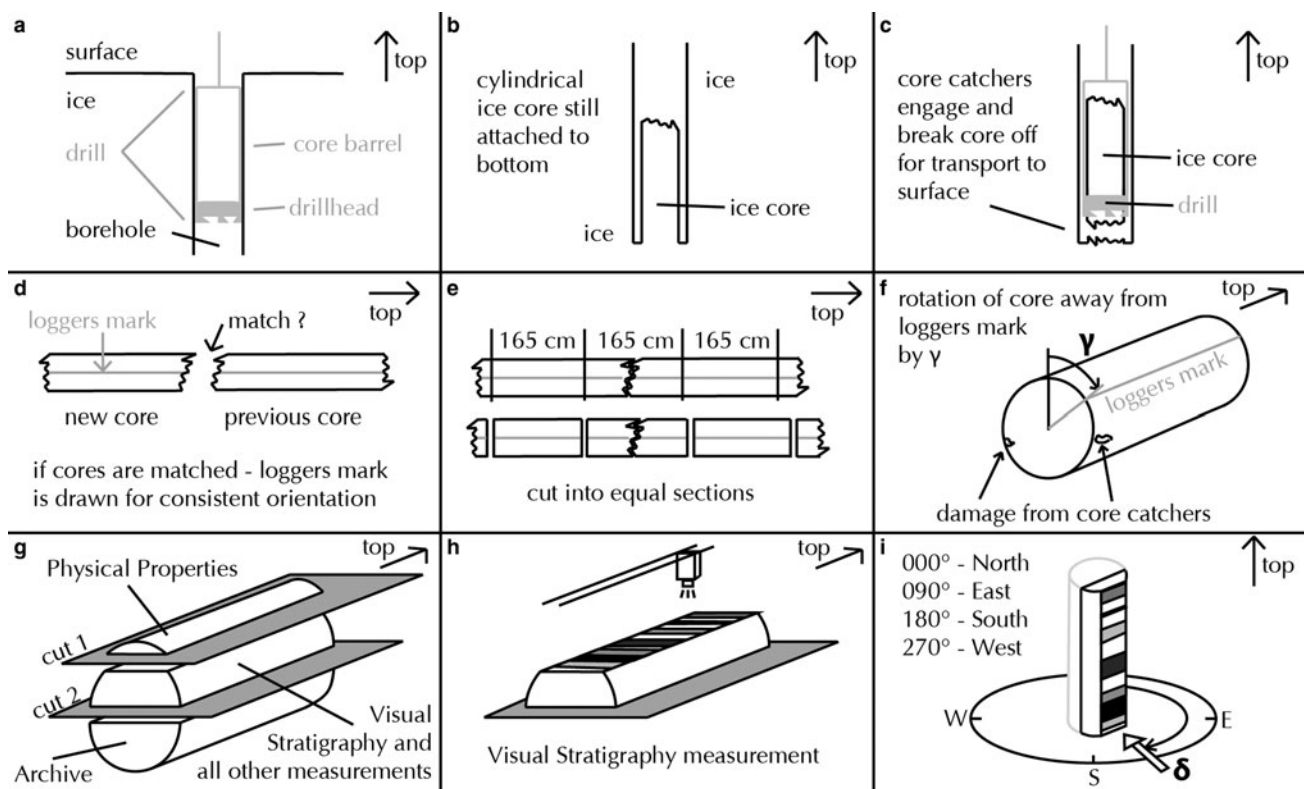


Fig. 2. Steps to recover an ice core until the measurement of visual stratigraphy (a to h). Spatial orientation of the direction of view, defined here as δ , is measured clockwise from North (i).

still attached to the bulk ice (Fig. 2b). The core catchers engage the ice, and the pull of the winch breaks the cylinder of ice off the bottom. The length of this cylinder, obtained in one run, can be up to 3.6 m, depending on core barrel length. It is then lifted to the surface (Fig. 2c), while the drill and core barrel rotate freely, and the in-situ core orientation is lost.

When the core reaches the surface, its top is matched to the bottom break of the previous ice core section (Fig. 2d). In most cases, this match is possible, thus retrieving the relative orientation of the drill core. The logger's mark, a continuous line on the core, represents this relative orientation. For ease of handling, the core is cut into regular sample lengths, e.g. 165 cm pieces at EastGRIP (Fig. 2e).

In cases of shattered ice, core quality is affected and samples are rotated to provide undamaged ice for all necessary measurements. It is rotated relative to the line marked on the core (γ , Fig. 2f).

Now two cuts are made along the long axis of the core (Fig. 2g). This provides three 165 cm-long pieces, one for physical properties measurements, one for visual stratigraphy and most other measurements, and one as an archive piece for future purposes. The visual stratigraphy sample is created by an optical 2D scan from the top (Fig. 2h) while being illuminated from below. Figure 2i illustrates the spatial orientation of the ice core, described as δ from now on. It is measured clockwise from geographic North.

2.2 The line scanner

The line scanner, used at EastGRIP, has been developed by Schäfer+Kirchhoff GmbH, in cooperation with Alfred Wegener Institute, Helmholtz Centre for Polar and Marine Research (AWI). Details can be found in, e.g. Svensson and others (2005) or Faria and others (2018). On Greenland, the line scanner was applied to obtain a line scan profile for sections of the NEM

deep ice core during the field campaign seasons 2009 to 2011 (unpublished data). An older version of this device was used for the drilling campaign at the Northern Greenland Ice Core Project (NorthGRIP), in the 2000s Svensson and others (2005). At NorthGRIP, the line scan was only done on the second NorthGRIP core, below 1300 m. The first visual archives of an ice core from Greenland were created on the Greenland Ice Core Project (GRIP) and the Greenland Ice Sheet Project (GISP2) ice cores in the 1990s, in an enormous effort, using pencil and paper (Grootes and others, 1993; Alley and others, 1997).

Faria and others (2010) and Jansen and others (2016) show the potential of visual stratigraphy images, e.g. complementary to other methods for deciphering deformation mechanisms, novel for identifying structures in ice such as tilted-lattice bands. Other applications are stratigraphic dating of ice cores, as done by, e.g. Svensson and others (2005).

To acquire the line scan images, a polished slab of ice is illuminated at an angle from below, often referred to as 'dark field' imaging. Impurities, dust, bubbles, and fractures will scatter the light, thus making these features visible. While the core is illuminated, a camera scans the surface and detects areas where light is scattered (Fig. 2h). Where light travels through 'clean' ice and is not scattered, a dark field below the ice core is detected (Svensson and others, 2005; Faria and others, 2010). The main cause of light scattering in ice from the last glacial period, other than fractures, is cloudy bands. These are layers with a high mineral dust concentration (Hammer and others, 1978), and micro-inclusions (Faria and others, 2010).

2.3 Borehole logging

The Danish Borehole Logger (Gundestrup and others, 1994) provides the boreholes inclination and spatial azimuth orientation. The inclination (i) of a borehole can be defined as the angle

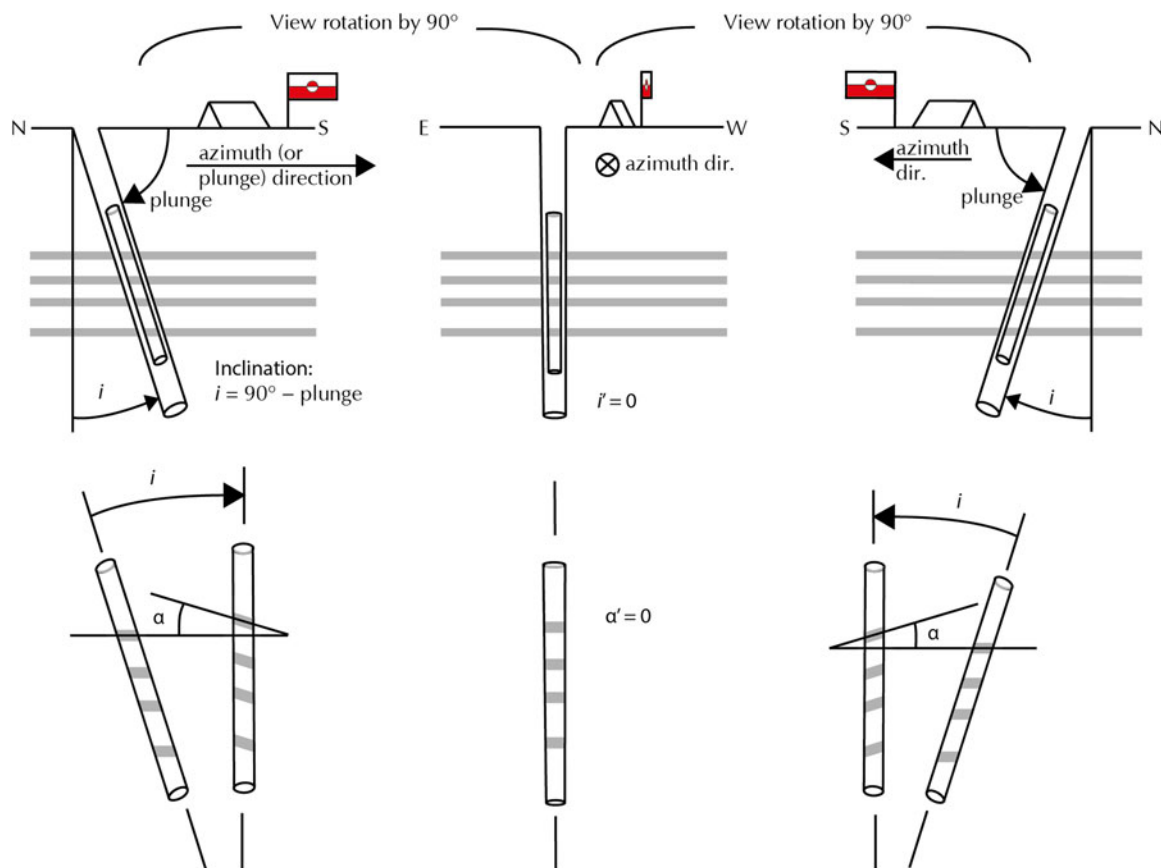


Fig. 3. Three viewing directions of the same borehole. In the top row, the angles i and i' represent the true and apparent borehole inclination ($90^\circ - \text{plunge}$), respectively. i and i' in the bottom row are the angles necessary to tilt the ice core to vertical. Assuming horizontal layering, i is equal to α , the dip angle of inclined layers in the ice core and i' is equal to α' , the apparent dip angle.

between the vertical and the borehole axis, or its plunge, which is the angle it makes with the horizontal plane (Fig. 3). The plunge (or azimuth) direction is the geographic direction in which the borehole points when projected on the horizontal plane. For consistency, we will from now on refer to plunge direction as azimuth direction (φ). We use the convention that $N = 000^\circ$, $E = 090^\circ$, etc., up to $360^\circ = 000^\circ$ (Fig. 2i).

In this study, we do not include other measurements by the logger (temperature, borehole diameter, and liquid pressure). The EastGRIP borehole has been drilled with inclinations up to 6° from vertical. The borehole is logged at the beginning and end of every field season with the purpose of observing undisturbed borehole temperatures, changes of diameter, and borehole geometry due to ice deformation. The measurements from the end of the 2019 field season are used here.

2.4 Tilt of cloudy bands due to borehole tilt

An observer looking at an arbitrarily oriented borehole will see an apparent inclination of $i' = 0^\circ$ (or a vertical plunge of 090°) when looking in the borehole azimuth direction, or in the opposite direction (Fig. 3 middle). Any other viewing direction results in an apparent inclination between 0° and the true inclination, when the viewing direction is $\pm 090^\circ$ to the azimuth direction ($i' = i$, Fig. 2, left and right). The same is observed when considering the tilt of layers (usually cloudy bands) in an extracted drill core.

The orientation of the true horizontal plane in a core is not known if the core is not oriented and, therefore, only its inclination and azimuth direction are known. We therefore define the horizontal in a core as the plane perpendicular to the core axis. When the core transects layering at an angle less than 090° ,

layering will appear tilted. The true tilt α will only be observed when looking at the core perpendicular to the material line in the core that was originally parallel to the plunge direction. The observed tilt α will then be identical to i , but with opposite sign. Here we use the sign convention that α is positive when layers appear to be tilted clockwise, i.e. to the right. When the core is observed from an arbitrary direction, the layers will have an apparent tilt angle α' , which can range from $-i$ to $+i$.

2.5 Measuring a cloudy band's tilt

We automatically measured the layer tilt of all 451 visual stratigraphy samples (equivalent to 745 m of core) using Matlab (MATLAB, 2018). Other methods for measuring a layer's tilt are discussed later. We created a brightness-intensity profile along the left and right sides of each image. Bright sections caused a peak in the signal and dark sections valleys. Using the built-in function for signal processing, 'alignsignals' the offset (D) of the left and right brightness-intensity curves was determined. With a known distance between the left and right side (x), the angle is calculated with simple trigonometry:

$$\alpha' = \tan\left(\frac{D}{x}\right). \quad (1)$$

Manual verification was necessary because irregularities in the layers may prevent the proper alignment of the same layer. In the samples, we observe three types of layering. Straight, regular layers with (Fig. 4a), long wavelength undulations (Fig. 4b), and small-scale folds with approximately vertical axial planes, termed crenulations in geology (Cosgrove, 1976, Fig. 4c). Crenulations

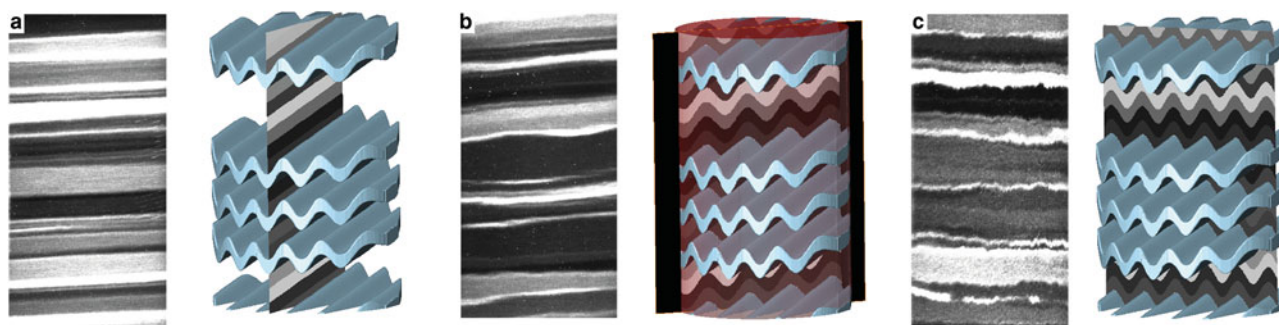


Fig. 4. Three types of deformation features. (a) No features and flat layering, (b) long wavelength undulations, and (c) crenulations (symmetric upright folds), overprinting other features. Visible structures depend on direction of view, illustrated by the cylinder with several folded layers next to every image.

form by lateral shortening of thin laminations in rocks or a foliation defined by strongly anisotropic minerals, such as micas (Cosgrove, 1976; Ran and others, 2019) or ice (Bons and others, 2016).

The automated method for tilt measurements was verified manually on 30 random samples. It provides good ($\pm 0.1^\circ$) results on featureless layers (Fig. 4a), but the measured tilt scatters in case of samples with folded or undulating layers (Fig. 4b). Using the median of up to 288, tilt measurements on one sample delivered results very similar (within $\pm 0.3^\circ$) to manual measurement. All angles greater than 8° (or smaller than -8°) were removed after manual verification that no layers have such a large inclination.

2.6 Reconstructing the core orientation

Figure 5 illustrates terms explained in the following section. The tilt or dip direction (labeled as ‘dip dir’) is the direction of the steepest inclined line on a tilted plane. The dip angle (α) is the declination of this plane, measured from a horizontal projection (\overline{MA}). The angle α is the largest possible plunge angle of a line on this plane. Strike is the unique non-inclined line on an inclined plane. Dip direction is 90° to strike and when viewed from the top, as in Fig. 5a (right), \overline{MA} and ‘dip dir’ have the same orientation.

The apparent dip (α') is the dip angle that is actually observed when a core is sectioned. Apparent dip direction (Fig. 5, red line $\overline{MA'}$) is the geographic orientation of this intersection on a horizontal plane. α' ranges between α and 0 (absolute values). For further details about apparent dip consult, e.g. Fossen (2016). The dip direction relative to strike, of any apparent dip angle α' is given by β :

$$\sin(\beta) = \frac{\tan(|\alpha'|)}{\tan(\alpha)}. \quad (2)$$

In our case, α is given by the maximum inclination of the borehole (i , Fig. 3) and α' represents the measured tilt of a cloudy band in a visual stratigraphy sample. The angle β is defined as the angle between the strike and the intersection of the section and horizontal plane, $\overline{MA'}$ (red line in Fig. 5). It is also the angle between strike and $A'B'$ and $A''B''$. The lines $A'B'$ and $A''B''$ extended as planes parallel to the ice core axis, and are two possible section orientations for a given angle β (Fig. 2g). Visual stratigraphy is scanned from a 90° angle to the section plane (Fig. 2h). For such a given angle β , these two planes can be viewed from two opposite directions, giving a total of four possible viewing directions $\delta_{(1-4)}$:

$$\delta_{(1,2)} = \varphi + 90 \pm (90 - \beta), \quad (3)$$

$$\delta_{(3,4)} = \varphi - 90 \pm (90 - \beta). \quad (4)$$

The borehole azimuth direction (φ) was logged at the end of the 2019 field season and is required to determine the other angles that link the coordinate system from Fig. 5 to a fixed geographical orientation, as in Fig. 3.

$\delta_{(1,2)}$ have a positive layer tilt (downward sloping to the right), both are on the $+90^\circ$ side in Fig. 5, bottom panel. Negative tilts (to the left) are represented by $\delta_{(3,4)}$, lying on the -90° side. Knowing the sign of the layer tilt reduces the number of possible orientations from four to two, as either Eqn (3) or (4) would apply.

We will show that $\delta_{(1,2)}$ (or $\delta_{(3,4)}$) are connected to the type of deformation structure seen in the visual stratigraphy. This makes each δ unique to distinguish and enables the reconstruction of the true direction of view.

3 Results

3.1 Input parameters for EastGRIP core orientation reconstruction

The analyzed samples range from a depth of 1375 to 2120 m. We measured the tilt of cloudy bands (α') for every visual stratigraphy sample, and plot one point per 165 cm-long sample (Fig. 6a). Measured layer tilts vary between -4° and $+4^\circ$, and are randomly distributed. In Fig. 6a, some clusters are visible and these will be discussed later.

The borehole inclination i ranges from 2.7° to 3.6° (Fig. 6b). Assuming horizontal layers in the ice sheet, i of the borehole is equal to the maximum layer tilt α in the ice core (Fig. 3). For $i = 3.5^\circ$, we expect to see an apparent layer tilt α' ranging from 0 to $\pm 3.5^\circ$, depending on the viewing direction.

In the analyzed depth range, the borehole azimuth direction ranges from 190° to 150° , meaning it shifts from plunging towards south to a southeast direction (Fig. 6c). This information is the input for Eqns (3) and (4) to retrieve an absolute orientation for the ice core.

3.2 Deformation structure matched to layer tilt

To differentiate the two potential δ , we make use of observed deformation structures, as explained above (Fig. 4). When plotting the cloudy band's inclination against depth, color-coded for specific deformation structures, a systematic arrangement is visible (Fig. 7). Above 1900 m, the flat layers with no features (Fig. 7a, mean as dashed line) are located at the high and low values of the tilt. In the same depth range, cloudy bands with crenulations (Fig. 7c) have values closer to 0° . Cloudy bands with

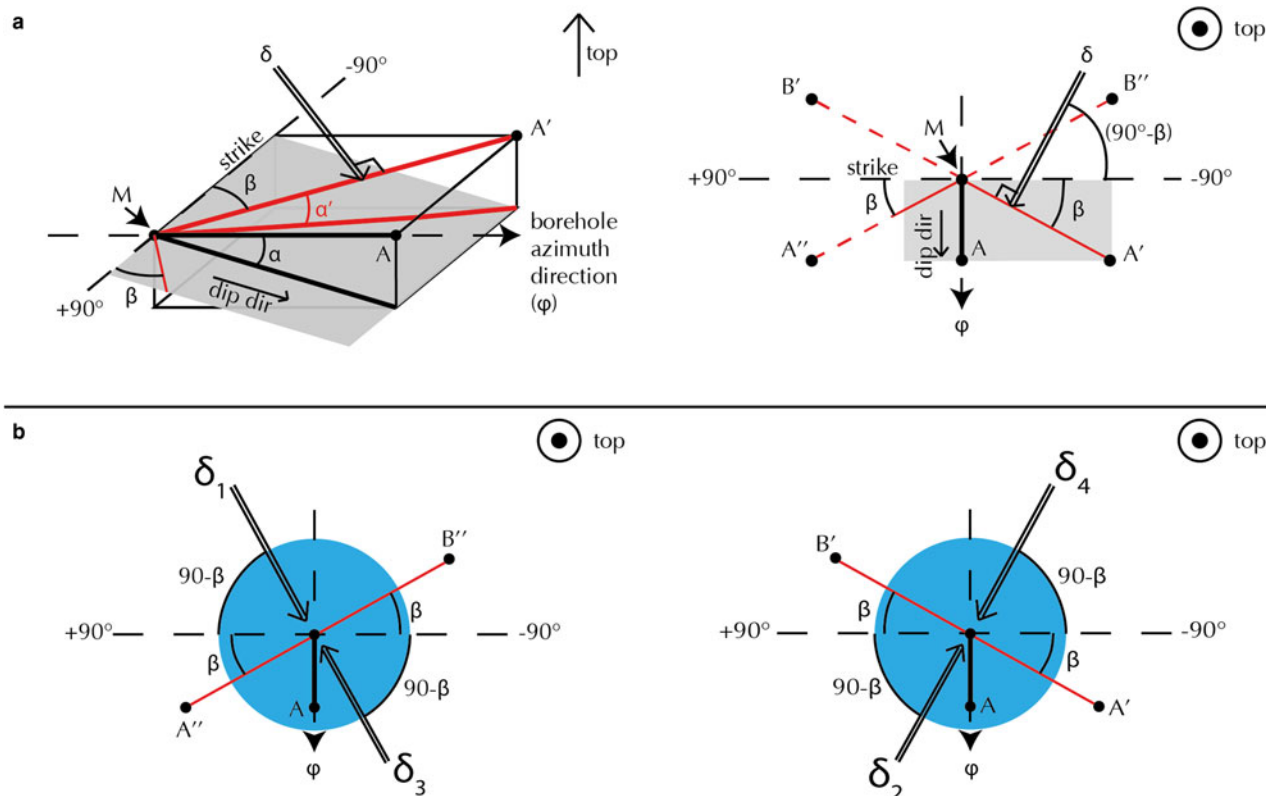


Fig. 5. (a) An inclined plane (gray square), e.g. a layer in an ice core, with the dip angle α on the steepest profile \overline{MA} . Same dip of gray layer, but smaller apparent dip angle α' on profile $\overline{MA'}$. Profile $\overline{MA'}$ is β away from strike. For one apparent dip angle α' there are four possible positions for β , spanning profiles from M to A', A'', B', and B''. (b) Ice core (blue circle) viewed along the vertical axis. Surface of 'cut 2' (Fig. 2G) is either along $\overline{A'B'}$ or $\overline{A''B''}$. $\delta_{(1-4)}$ represent the possible viewing directions. All red lines, extended vertically, could be possible image planes.

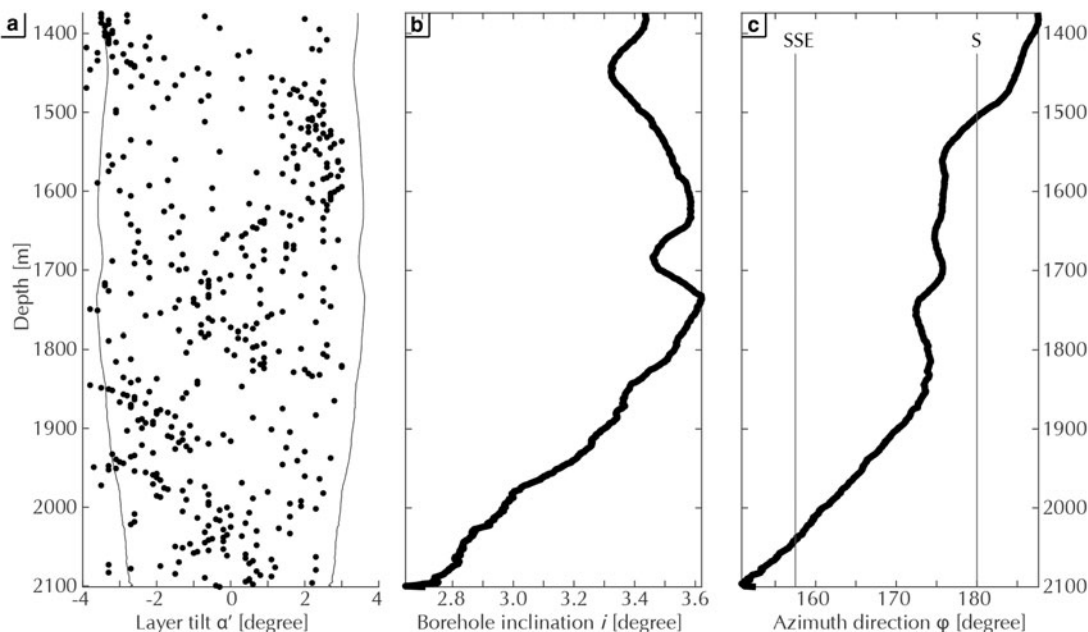


Fig. 6. (a) Tilt of cloudy bands (α') from 1375 to 2120 m (bag 2500 to 3856), each circle is the median value of 288 measurements for each 165 cm-long sample. (b) Inclination i and (c) azimuth direction φ of the EastGRIP borehole against depth. Inclination angle from (b) also shown as a thin line in (a).

long-wavelength folds and undulations (Fig. 7b) scatter over the full spectrum of layer tilts.

Borehole inclination and azimuth direction change significantly below 1900 m (Fig. 6). The tilt of layers with no features (Fig. 7a) gradually shifts to values around 0°. Layers with crenulations (Fig. 7c) now incline at larger values. Thus, these specific deformation features are linked to specific layer tilts.

3.3 Work flow diagram

The flow diagram (Fig. 8, left side) supplies the user with a step-by-step instruction on how to use the presented method. It requires the input of borehole geometry (#1) and visual stratigraphy images (#2), and knowledge about ice flow direction (step 5). All other parameters are obtained from these. In the

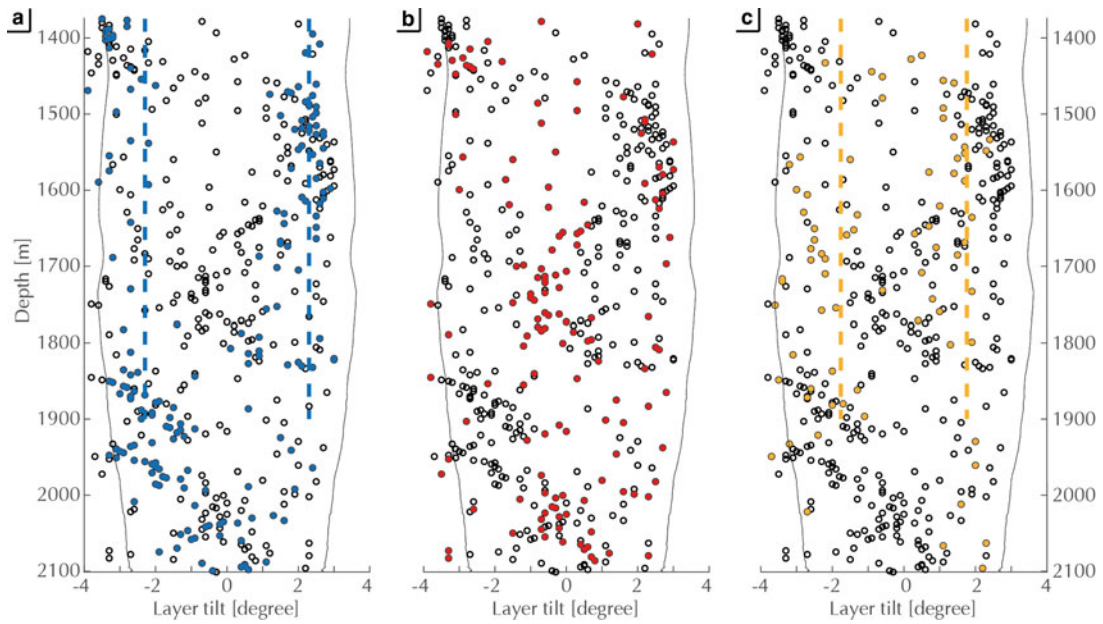


Fig. 7. Deformation-structure types and the corresponding layer tilt of cloudy bands against depth. Cloudy bands with no or flat features (a, blue), long wavelength undulations and folds (b, red), and crenulations (c, orange). Dashed lines are means for 1375 to 1900 m separated for positive and negative tilt. No features mean: ± 2.3 and crenulations mean: ± 1.6 .

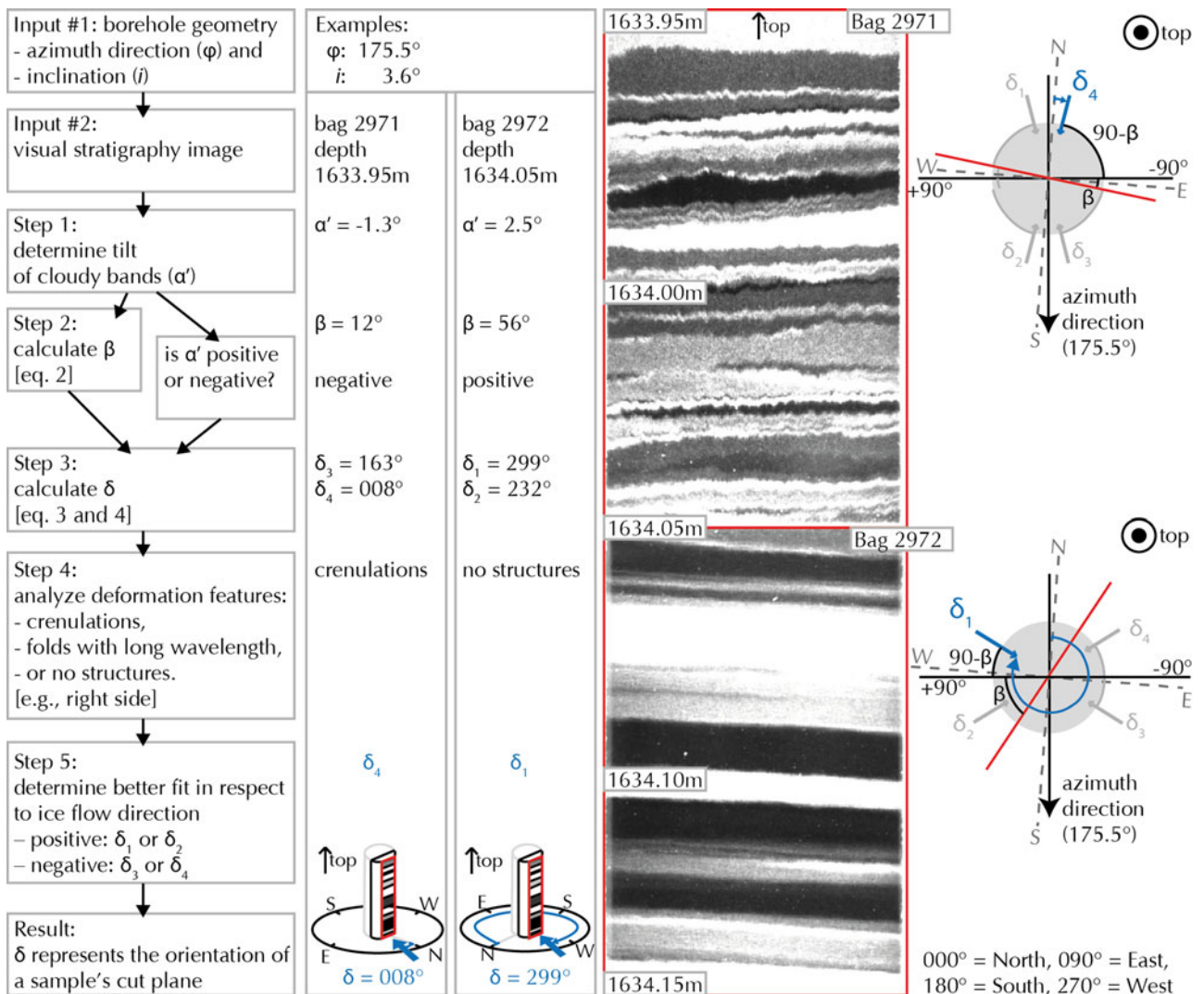


Fig. 8. Left: flow diagram to determine ice core absolute orientation, applied on bag 2971 and 2972. Middle: visual stratigraphy images of the two consecutive bags, including a depth scale. Right: sketch of visual stratigraphy plane, including relevant angles to obtain the orientation. Blue: spatial orientation of δ . Red: visual stratigraphy plane.

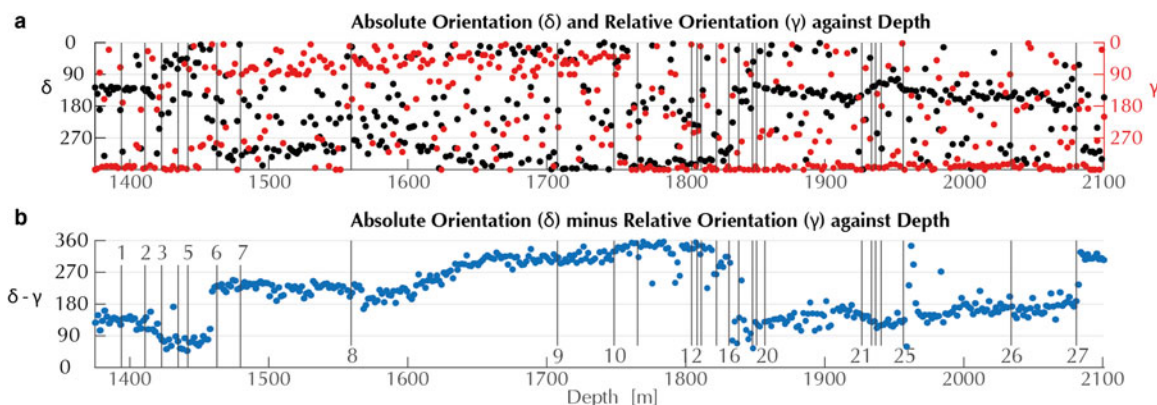


Fig. 9. (a) Absolute spatial orientation δ (black) and relative orientation γ (red) against depth. (b) $\delta - \gamma$ (blue) describes the offset angle of the relative orientation from geographic North. Vertical lines show core breaks where a match was not possible.

following, to illustrate the method, two consecutive visual stratigraphy images from a depth of around 1634 m (bag 2971 and 2972), with different deformation structures, are compared and reoriented (Fig. 8, right side).

Input #1 defines the reference system, i.e. the azimuth direction and inclination of the borehole. Azimuth direction φ is 175.5° , and borehole inclination i is 3.6° for bag 2971 and 2972. Thus, this is also the dip direction and dip angle of our layers.

The apparent dip α' , i.e. the visible tilt of the layers, in bag 2971 and 2972 is -1.3° and 2.5° , respectively. We apply Eqn (2) to calculate β , which is 12° and 56° , respectively. For a negative layer tilt α' , Eqn (4) is used for bag 2971. For the positive tilt α' in bag 2972, we apply Eqn (3). Both provide two possible viewing directions $\delta = 008^\circ$ and $\delta = 163^\circ$ for bag 2971 and $\delta = 232^\circ$ and $\delta = 299^\circ$ for bag 2972 (see Fig. 8).

In the visual stratigraphy of bag 2971, we can clearly identify crenulations, linked to compression folds, and thus, the direction of view for δ must be close to perpendicular to ice flow direction of NEGIS (flow towards 025°). In this case, the position at 008° fulfills this requirement. A viewing direction of 163° would not represent an angle where compressional folds would be visible in the stratigraphy, and can therefore be eliminated as a possible viewing direction.

Cloudy bands in bag 2972 show no deformation features. Thus, the cut plane must be oriented approximately parallel to flow direction. At $\delta = 232^\circ$, we would expect to see deformation features in the cloudy bands. The second option $\delta = 299^\circ$ however, is closer to the anticipated value parallel to the ice flow direction. Therefore, the first value (232°) can be ruled out.

3.4 Comparison of viewing direction δ to other methods

3.4.1 Relative orientation from core recovery

Before cutting the ice core for visual stratigraphy analysis, it is rotated at an angle γ , relative to the loggers mark (illustrated in Fig. 2f). This rotation defines the relative core orientation γ , which is continuously documented (Fig. 9, red). We calculate the absolute orientation δ (Fig. 9, black) for all samples, which represents the orientation relative to geographic North. We observe a strong correlation in the difference of absolute and relative orientation $\delta - \gamma$ (Fig. 9, blue). Subtracting γ from δ determines the deviation of the loggers mark from geographic north (compare to Fig. 2).

Figure 9 also indicates the loss of relative core orientation (vertical black lines) due to mismatches of core breaks (illustrated in Fig. 2d). For each mismatch in a core break, a new loggers mark is created, which has a random but continuous

orientation for a range of matching core breaks. In sections with a preserved relative core orientation, very small rotations (of γ) are aimed for prior to cutting the ice core for visual stratigraphy. This results in many layer tilt measurements clustering around a certain value as this is the preferred cut orientation during core preparation.

All core mismatches in this section are documented in the field protocol as 'probably lost', except break number three, 16, and 19, which are labeled as 'not-matched'. 'Not-matched' means that the relative orientation is lost, but the mismatches at breaks three and 19 do not show this mismatch in our data (Fig. 9). On the other hand, the mismatch at break 16 is clearly visible. In many of the assumed core mismatches, the orientation is, in fact, not lost (e.g. break one, seven, nine, and 26). A prominent example of a loss of core orientation is break 27, where the orientation ($\delta - \gamma$) changes abruptly.

3.4.2 Orientation of crystal-scale directional features

The orientation of a single ice crystal can easily be described by its c -axis, which is the vector perpendicular to the crystal's basal plane (e.g. Petrenko and Whitworth, 1999). C -axis orientation has been measured continuously, every 10–15 m, throughout the EastGRIP core. Between 1375 and 2120 m, we use 34 c -axis plots. They show a c -axis distribution that is classified as a girdle in varying strengths.

Each projection alone shows a developed girdle with various orientations (Fig. 10a). These plots have a random orientation, when all are plotted together without rotational correction (Fig. 10b₁). This is also visible in the rose diagram and histogram (Fig. 10b_{2,3}). Each c -axis plot may be rotated by δ as determined by the method reported here (Fig. 10a). A systematic directional feature, i.e. a girdle with the same orientation for all samples, is visible when all samples are oriented (Fig. 10 bottom panel). The vertical girdle is now clearly orientated towards 120° and 300° , which is approximately perpendicular to the assumed flow direction at 030° .

4 Discussion

4.1 Statistical overview

Reorientation of the EastGRIP ice core worked well for 396 of 451 samples (88%). These 451 samples cover 745 core meters, which covers the full interval of interest from 1375 to 2120 m depth. After a comparison with the relative orientation γ , a good agreement was found for 441 of 451 samples (98%). In the remaining ten samples, the layer tilt is very close to 0° , so the sample can be

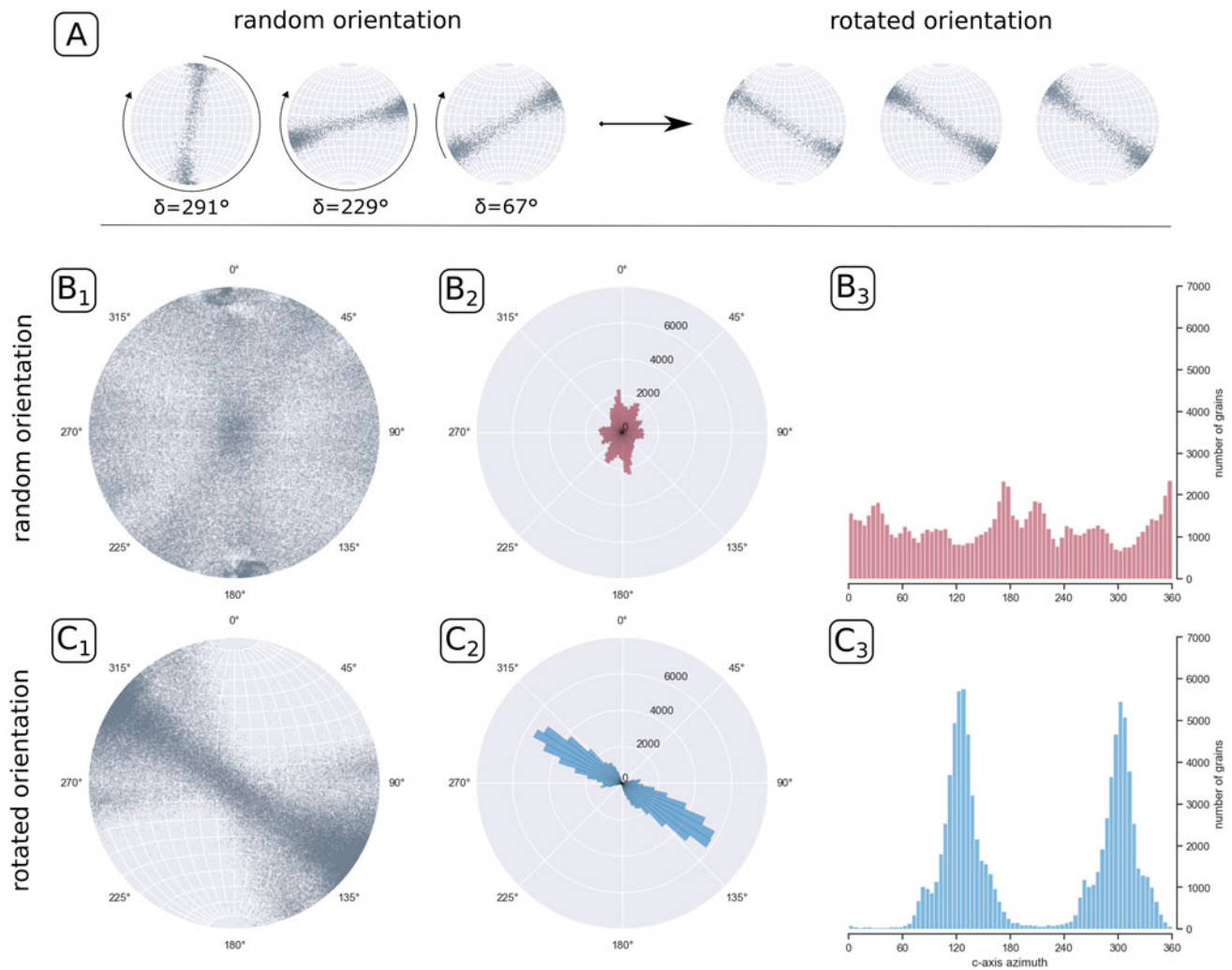


Fig. 10. Comparison of stereographic projections of crystallographic oriented fabric c-axis of an unrotated and rotated ice core. Panel (a) shows three individual stereographic projections before and after the rotation. A comparison of 34 c-axis data sets are shown in panels (b) and (c), with: (1) stereographic projections of the c-axis of all ice crystals, (2) a rose diagram, and (3) a histogram showing the distribution of the azimuth of all ice crystals binned in 5 degree units, respectively, before and after re-orientation.

viewed from two opposing sides, allowing two possible orientations, which cannot be distinguished further.

4.2 Cloudy band tilt measurement

The limited accuracy in measuring the inclination of a cloudy band is the largest source of uncertainty. The measurements in featureless samples are the most accurate, as every cloudy band is parallel to the one above and below.

As deformation of the visual stratigraphy increases, the accuracy of the tilt measurement declines. The approach by Drews and others (2012), who used the Hough transform (Hough, 1962) on visual stratigraphy data from the European Project for Ice Coring in Antarctica, Dronning Maud Land Deep Drilling (EDML), was tested on our data. We added a pre-processing step to the Hough transform, using the built-in Matlab skeleton function for binary images, which greatly improved the outcome (MATLAB, 2018). The skeleton function finds the centerline between two edges, providing the average tilt of the top and bottom edge of a cloudy band. Still, a large number of detected lines in the image did not match stratigraphic layers. Therefore, for our approach, we determined a cloudy band's inclination by using left-right grayscale signal alignment (see method section).

Another approach for detecting the layer tilt is using fast Fourier transform. This method is suggested by McGwire and

others (2008) and applied on the West Antarctic Ice Sheet Divide Deep ice core (Fitzpatrick and others, 2014). However, it holds the same limitations as the Hough transform and our grayscale alignment, as undulations and folds in the cloudy bands scatter the result.

An increase of disturbances in the cloudy bands correlates with variations of layer tilt within one sample. The top edge of a cloudy band can have a different tilt to the bottom one, as the layer thickness can vary within the width of one sample (Fig. 8, cloudy band at 1633.98 m). This means that any method to determine layer tilt will suffer an increase in uncertainty the more the layers are disturbed. We therefore assume that the straightforward comparison between left and right sides of a sample suffices.

4.3 Relative and absolute orientation

To estimate the uncertainty in the tilt measurement, we compare the absolute orientation δ to the relative orientation γ . The latter was collected over three field seasons, by approximately nine different operators, and rounded to the next 5° or 10°, therefore, we expect a certain range of scattering. Figure 9b shows that the difference of absolute orientation minus relative orientation ($\delta - \gamma$) align. If we assume γ to be very precise (to the closest 5°), the noise in this alignment is caused by inaccuracies in δ . Although there are uncertainties in tilt measurements of cloudy bands,

the results show that the general orientation δ agrees with the relative orientation γ taken during ice core processing in the field.

The presented results are a rare opportunity to analyze the quality of core break matching (Fig. 2d) during ice core logging in the field. Mistakes made can be identified by comparing the relative orientation γ (Fig. 2f) to the absolute orientation δ . A loss of relative core orientation is indicated as a sudden change of $\delta - \gamma$. Three of these are easily spotted between break five and six, at break 16, and break 27. While break 16 and 27 are located exactly at the change of angle, the change of angle at 1459 m depth is located 4 m above mismatch six. As this agrees well with the length of core retrieved in one drill run, we can interpret an inconsistency in documenting the depth while logging. This interpretation is most likely not valid for mismatch eight, where the small change in $\delta - \gamma$ is observed 7 m deeper.

An interesting feature is the slow shift of $\delta - \gamma$ between 1600 and 1650 m (from 210° to 300°). The relative orientation is assumed to have been kept constant and borehole inclination and azimuth barely change (Fig. 6). However, an observed gradual shift over 90° could be the sum of tiny shifts in orientation during ice core logging. We find inconsistencies in the loggers field protocol for this depth range, where although all core breaks are labeled as matched, smaller core sections are missing or out of place. This gradual shift of relative orientation could be the result of small core break mismatches, due to these missing or too small sections. A more abrupt change in $\delta - \gamma$ is observed between mismatch 11 and 12, where $\delta - \gamma$ decreases sharply and then returns to the previous level. Again, the loggers field protocol shows inconsistencies for this part of the core, however, without mentioning further details. We argue that the deviations of five samples after mismatch 25 are most likely related to an incorrect measurement of γ because the correlation works well before and after this section and no errors in the tilt measurements were found.

Problems with core break matching seem to cluster. They are located between mismatch 12 to 20 and 21 to 25. While this could be related to variations in the drill setup and difficulties in drilling, leading to a reduced core quality, it could also be related to personal preferences of the core logging operators.

In the cluster between mismatch 12 and 20 there are several occasions where a mismatch was assumed, but the orientation was actually preserved, e.g. at mismatches 12, 13, 14, and 20. The challenges for continuous and precise core break matching can be observed between mismatch 15 and 19, where the values show a large variability and two mismatches are labeled as 'not-matched'.

There are many sections where core break matching worked very well. Between mismatch seven and eight, 20 and 21, and 25 and 27, $\delta - \gamma$ does not change over longer periods. Even with a number of different personnel acquiring the data, core break matching works very well in the analyzed depth region. The field protocol seems to be more on the conservative side, as at most of the mismatches labeled with 'probably lost' the relative core orientation is actually preserved. Also, the documentation of core rotation prior to cutting (γ , Fig. 2f) was done in an diligent manner, with very few exceptions.

4.4 Direction of flow inferred from the crystal orientation

The orientation distribution of the c -axes of crystals in one sample are called fabric, or crystal preferred orientation (CPO). When ice is deformed, the CPO changes, with its type depending on the dominating deformation mode (e.g. Kamb, 1972). The two main processes impacting the fabric pattern are (1) rotation of c -axes towards the direction of maximum finite shortening (Alley, 1992; Qi and others, 2019) and (2) recrystallization leading to the formation of new grains with different orientations,

compared to the host grain (Llorens and others, 2017). Information on the deformational history can therefore, to a certain extent, be derived from the fabric of a sample (Kamb, 1972; Thorsteinsson and others, 1997; Wang and others, 2002; Montagnat and others, 2014; Weikusat and others, 2017).

According to Cuffey and Paterson (2010), the observed developed vertical girdle between 1375 and 2120 m indicates extensional deformation along flow direction. If the dominating stress regime is axial extension, crystals rotate and basal planes shift towards parallelism with the direction of extension (Thorsteinsson and others, 1997; Wang and others, 2002). Hence, c -axes rotate away from the direction of extension, producing girdle fabrics. Depending on their strength, patterns are classified as developing, developed, or strong girdle. The stronger a girdle, the more c -axes are aligned in the girdle, and the thinner the girdle becomes (Cuffey and Paterson, 2010).

The use of visual stratigraphy data enabled us to rotate the c -axis orientation data in a structured way. Doing so results in girdles that are aligned perpendicular to the observed flow direction of 030° of NEGIS. Our data confirm that the ice stream's extensional deformation results in a vertical girdle perpendicular to the flow direction.

Some scatter remains, which can be explained by unavoidable difficulties in measuring the angle of undulations and folds in stratigraphic layers and small-scale changes in the crystal fabric. However, the rotation of the fabric data using the correction we derived with our method turned out to be successful and indicates a deformation pattern, which agrees very well with the observed flow direction of NEGIS (Hvidberg and others, 2020).

4.5 Interpretation of visible deformation structures

The schematic image of folds in a cylinder, as done in Fig. 4, is an idealization, as it shows the gray-scale variation within an infinitely thin slice. Ice is a transparent material, and the image obtained in a line scanner is the product of light passing through a thick slice and is averaged over the focus depth. The sharpest image is obtained when layer boundaries align in the direction of observation. This is always the case in undisturbed layers. However, when layers are folded, this is only the case when looking along the fold axes. We therefore only observe sharp, thin layers with clear crenulation folds in sections at a large angle (δ around 025° or 205°) to the fold axis or extension direction. Cutting the folds obliquely results in more wavy patterns that may resemble extensional structures, such as boudins, shear bands, and truncations.

Field geologists are acutely aware that structures may look very different, depending on how they are intersected by the outcrop surface. The true nature and style of folds, for example, is only seen in surface that are approximately perpendicular to the fold axis. The same applies here. After having established the true orientation of all drill-core section, assuming a consistent fold-axis orientation, those sections that have the proper orientation can be selected to analyze the deformation structures. Care should be taken not to over-interpret other sections, as the oblique sections through structures may be misleading. A variation of cloudy-band morphology with depth could reflect a true variation in type or frequency of deformation structures. However, orientation of the drill-core sections should first be carried out to ascertain that this is not an artifact of sectioning. In the current case, it appears that variations that range from straight layers to folds can be explained by this sectioning effect. Approximately straight layering is observed in sections close to parallel to the flow direction, while folds are observed in those perpendicular to it. This is consistent with extension of the ice sheet in the direction of flow and lateral constriction, which is expected to result in the observed fold orientations (Bons *et al.*

2016). The surface velocity fields at the EastGRIP drill site (Hvidberg and others, 2020) support this deformation regime as surface flow lines converge into the ice stream. Inside NEGIS the ice flow is parallel and the velocity is a magnitude higher than outside of the stream. Velocity at EastGRIP increases downstream, implying extension in the flow direction.

5. Conclusions

We present a simple method to determine the in-situ orientation of an ice core (summarized in a flow chart in Fig. 8). Knowledge of this orientation of an ice core sample and the associated orientated physical properties is a major advance for the interpretation of deformation structures. Macroscopic folds in the visual cloudy-band stratigraphy, as well as deformation-related micro-structures and crystal fabrics can now be described with consideration of their spatial orientation. This leads to a high gain in information about the direction in which ice deforms and how it flows. This will greatly facilitate and improve the interpretation of deformation structures and the kinematic framework of that deformation.

This method contributes to the application of computational models, as visible 3D structures from the ice core are now comparable to the result of 3D models. This is possible as the direction of view δ covers the full 360° of possible orientations, so throughout core depth every direction is visible with its corresponding deformation structures. Using many 2D images, with different orientations, the 3D structure of an ice core can now be constructed.

Including other methods, such as analyzing the crystal-fabric orientation, we can further improve this method and enhance the accuracy. However, this study shows that the fabric is not a necessary input parameter for reconstructing the ice core orientation.

Information about ice core orientation is a necessity when interpreting structures seen in the ice core. This ranges from micro-scale features in the ice core lattice to macro-scale features seen in centimetre-scale folds. Neglecting the ice core orientation can lead to incomplete, and possibly misleading, interpretations of the physical processes related to ice flow and more generally, any analyses based on 2D images of an ice core.

Acknowledgments. We especially thank the logistics and drill team of the EastGRIP project, without you we wouldn't have the ice core. Thank you also to the ice core logging and processing teams, for your work and detailed documentation. Great thanks also to the physical properties processing team for generating the data. EastGRIP is directed and organized by the Centre for Ice and Climate at the Niels Bohr Institute, University of Copenhagen. It is supported by funding agencies and institutions in Denmark (A. P. Möller Foundation, University of Copenhagen), USA (US National Science Foundation, Office of Polar Programs), Germany (Alfred Wegener Institute, Helmholtz Centre for Polar and Marine Research), Japan (National Institute of Polar Research and Arctic Challenge for Sustainability), Norway (University of Bergen and Bergen Research Foundation), Switzerland (Swiss National Science Foundation), France (French Polar Institute Paul-Emile Victor, Institute for Geosciences and Environmental research) and China (Chinese Academy of Sciences and Beijing Normal University). We also thank the Villum Foundation, as this work was supported by the Villum Investigator Project IceFlow (NR. 16572). Thank you to the three anonymous reviewers for ideas on improving this manuscript. Special thanks to Pavel Talalay for the review and comments on drilling and core orientation. Many thanks also go to: Aslak Grinsted for ideas on measuring inclination angles, Anders Svensson for details on the historical background of the line scanner, and Paul Vallelonga for general support and discussions.

References

- Alley RB (1992) Flow-law hypotheses for ice-sheet modeling. *Journal of Glaciology*, **38**(129), 245–256.
- Alley R and 11 others (1997) Visual-stratigraphic dating of the gisp2 ice core: basis, reproducibility, and application. *Journal of Geophysical Research: Oceans*, **102**(C12), 26367–26381.
- Bons PD and 10 others (2016) Converging flow and anisotropy cause large-scale folding in Greenland's ice sheet. *Nature Communications*, **7**(1), 1–6. doi: [10.1038/ncomms11427](https://doi.org/10.1038/ncomms11427).
- Bons PD and 6 others (2018) Greenland ice sheet: higher nonlinearity of ice flow significantly reduces estimated basal motion. *Geophysical Research Letters*, **45**(13), 6542–6548. doi: [10.1029/2018GL078356](https://doi.org/10.1029/2018GL078356).
- Christianson K and 7 others (2014) Dilatant till facilitates ice-stream flow in northeast Greenland. *Earth and Planetary Science Letters*, **401**, 57–69, ISSN 0012821X, doi: [10.1016/j.epsl.2014.05.060](https://doi.org/10.1016/j.epsl.2014.05.060).
- Cosgrove J (1976) The formation of crenulation cleavage. *Journal of the Geological Society*, **132**(2), 155–178.
- Cuffey KM and Paterson WSB (2010) *The physics of glaciers*. Burlington, MA: Academic Press.
- Dansgaard W, Johnsen SJ, Møller J and Langway CC (1969) One thousand centuries of climatic record from Camp Century on the Greenland ice sheet. *Science*, **166**(3903), 377–380.
- Davis BK and Cowan E (2012) Oriented core—what the...? *Proceedings of the Structural Geology and Resources—International Symposium Abstract Volume, Australian Institute of Geoscientists, Perth*, pp. 61–63.
- Drews R and 5 others (2012) Potential mechanisms for anisotropy in ice-penetrating radar data. *Journal of Glaciology*, **58**(209), 613–624. doi: [10.3189/2012JofG11J114](https://doi.org/10.3189/2012JofG11J114).
- Fahnestock M, Abdalati W, Joughin I, Brozena J and Gogineni P (2001) High geothermal heat flow, basal melt, and the origin of rapid ice flow in central Greenland. *Science*, **294**(5550), 2338–2342. doi: [10.1029/2001JD900194](https://doi.org/10.1029/2001JD900194).
- Faria SH, Freitag J and Kipfstuhl S (2010) Polar ice structure and the integrity of ice-core paleoclimate records. *Quaternary Science Reviews*, **29**(1–2), 338–351. doi: [10.1016/j.quascirev.2009.10.016](https://doi.org/10.1016/j.quascirev.2009.10.016).
- Faria SH, Kipfstuhl S and Lambrecht A (2018) *Edml line-scan images*. In *The EPICA-DML Deep Ice Core*. Berlin Heidelberg: Springer, pp. 57–291.
- Fitzpatrick JJ and 11 others (2014) Physical properties of the WAIS divide ice core. *Journal of Glaciology*, **60**(224), 1181–1198. doi: [10.3189/2014JofG14J100](https://doi.org/10.3189/2014JofG14J100).
- Fossen H (2016) *Structural geology*. Cambridge: Cambridge University Press.
- Franke S and 7 others (2020) Bed topography and subglacial landforms in the onset region of the northeast Greenland ice stream. *Annals of Glaciology*, **61**(81), 143–153. doi: [10.1017/aog.2020.12](https://doi.org/10.1017/aog.2020.12).
- Gow AJ and Williamson T (1971) Volcanic ash in the antarctic ice sheet and its possible climatic implications. *Earth and Planetary Science Letters*, **13**(1), 210–218.
- Grootes PM, Stuiver M, White J, Johnsen S and Jouzel J (1993) Comparison of oxygen isotope records from the GISP2 and GRIP Greenland ice cores. *Nature*, **366**(6455), 552–554.
- Gundestrup NS, Clausen HB and Hansen BL (1994) The UCPH borehole logger. *Memoirs of National Institute of Polar Research*, **49**, 224–233.
- Hammer C and 5 others (1978) Dating of Greenland ice cores by flow models, isotopes, volcanic debris, and continental dust. *Journal of Glaciology*, **20**(82), 3–26.
- Hough PV (1962) Method and means for recognizing complex patterns. US Patent 3,069,654.
- Hubbard B and Malone T (2013) Optical-televiever-based logging of the uppermost 630 m of the NEEM deep ice borehole, Greenland. *Annals of Glaciology*, **54**(64), 83–89. doi: [10.3189/2013AoG64A201](https://doi.org/10.3189/2013AoG64A201).
- Hvidberg CS and 10 others (2020) Surface velocity of the NorthEast Greenland Ice Stream (NEGIS): assessment of interior velocities derived from satellite data by GPS. *The Cryosphere*, **14**, 3487–3502. doi: [10.5194/tc-14-3487-2020](https://doi.org/10.5194/tc-14-3487-2020).
- Jansen D and 7 others (2016) Small-scale disturbances in the stratigraphy of the NEEM ice core: observations and numerical model simulations. *The Cryosphere*, **10**, 359–370. doi: [10.5194/tc-10-359-2016](https://doi.org/10.5194/tc-10-359-2016).
- Johnsen SJ and 16 others (2007) The Hans Tausen drill: design, performance, further developments and some lessons learned. *Annals of Glaciology*, **47**, 89–98.
- Joughin I, Fahnestock M, MacAyeal D, Bamber JL and Gogineni P (2001) Observation and analysis of ice flow in the largest Greenland ice stream. *Journal of Geophysical Research: Atmospheres*, **106**(D24), 34021–34034.
- Joughin I, Smith B, Howat I, Scambos T and Moon T (2010a) *Measures Greenland ice sheet velocity map from InSAR data*. Boulder, Colorado:

- National Snow and Ice Data Center. doi: [10.5067/MEASURES/CRYOSPHERE/nsidc-0478.001](https://doi.org/10.5067/MEASURES/CRYOSPHERE/nsidc-0478.001).
- Joughin I, Smith BE, Howat IM, Scambos T and Moon T** (2010b) Greenland flow variability from ice-sheet-wide velocity mapping. *Journal of Glaciology*, **56**(197), 415–430. doi: [10.3189/002214310792447734](https://doi.org/10.3189/002214310792447734).
- Kamb B** (1972) Experimental recrystallization of ice under stress. *GMS*, **16**, 211–241.
- Llorens MG and 8 others** (2017) Dynamic recrystallization during deformation of polycrystalline ice: insights from numerical simulations. *Philosophical Transactions of the Royal Society A: Mathematical, Physical and Engineering Sciences*, **375**(2086), 20150346–doi: [10.1098/rsta.2015.0346](https://doi.org/10.1098/rsta.2015.0346).
- MATLAB** (2018) 9.7.0.1190202 (R2019b). Natick, Massachusetts: The MathWorks Inc.
- McGwire KC and 6 others** (2008) An integrated system for optical imaging of ice cores. *Cold Regions Science and Technology*, **53**(2), 216–228. doi: [10.1016/j.coldregions.2007.08.007](https://doi.org/10.1016/j.coldregions.2007.08.007).
- Mojtabavi S and 19 others** (2019) A first chronology for the East Greenland Ice-core Project (EGRIP) over the Holocene and last glacial termination. *Climate of the Past Discussions, in review*. doi: [10.5194/cp-2019-143](https://doi.org/10.5194/cp-2019-143).
- Montagnat M and 9 others** (2014) Fabric along the NEEM ice core, Greenland, and its comparison with GRIP and NGRIP ice cores. *The Cryosphere*, **8**, 1129–1138. doi: [10.5194/tc-8-1129-2014](https://doi.org/10.5194/tc-8-1129-2014).
- NEEM community members** (2013) Eemian interglacial reconstructed from a Greenland folded ice core. *Nature*, **493**(7433), 489–494. doi: [10.1038/nature11789](https://doi.org/10.1038/nature11789).
- Paulsen TS, Jarrard RD and Wilson TJ** (2002) A simple method for orienting drill core by correlating features in whole-core scans and oriented borehole-wall imagery. *Journal of Structural Geology*, **24**(8), 1233–1238. doi: [10.1016/S0191-8141\(01\)00133-X](https://doi.org/10.1016/S0191-8141(01)00133-X).
- Petrenko VF and Whitworth RW** (1999) *Physics of ice*. Oxford: OUP.
- Qi C and 8 others** (2019) Crystallographic preferred orientations of ice deformed in direct-shear experiments at low temperatures. *Cryosphere*, **13**(1), 351–371. doi: [10.5194/tc-13-351-2019](https://doi.org/10.5194/tc-13-351-2019).
- Ran H and 10 others** (2019) Time for anisotropy: The significance of mechanical anisotropy for the development of deformation structures. *Journal of Structural Geology*, **125**, 41–47. doi: [10.1016/j.jsg.2018.04.019](https://doi.org/10.1016/j.jsg.2018.04.019).
- Svensson A and 7 others** (2005) Visual stratigraphy of the North Greenland Ice Core Project (NorthGRIP) ice core during the last glacial period. *Journal of Geophysical Research: Atmospheres*, **110**(D2), 1–11. doi: [10.1029/2004JD005134](https://doi.org/10.1029/2004JD005134).
- Talalay P** (2014) Perspectives for development of ice-core drilling technology: a discussion. *Annals of Glaciology*, **55**(68), 339–350.
- Talalay PG** (2020) *Thermal Ice-Drilling Technology*. Singapore: Springer. doi: [10.1007/978-981-13-8848-4](https://doi.org/10.1007/978-981-13-8848-4).
- Thorsteinsson T, Kipfstuhl J and Miller H** (1997) Textures and fabrics in the grip ice core. *Journal of Geophysical Research: Oceans*, **102**(C12), 26583–26599.
- Vallelonga P and 22 others** (2014) Initial results from geophysical surveys and shallow coring of the Northeast Greenland Ice Stream (NEGIS). *The Cryosphere*, **8**(4), 1275–1287. doi: [10.5194/tc-8-1275-2014](https://doi.org/10.5194/tc-8-1275-2014).
- Wang Y and 5 others** (2002) A vertical girdle fabric in the northgrip deep ice core, north Greenland. *Annals of Glaciology*, **35**, 515–520.
- Weikusat I and 10 others** (2017) Physical analysis of an antarctic ice core—towards an integration of micro-and macrodynamics of polar ice. *Philosophical Transactions of the Royal Society A: Mathematical, Physical and Engineering Sciences*, **375**(2086), 20150347. doi: [10.1098/rsta.2015.0347](https://doi.org/10.1098/rsta.2015.0347).